A bipartite interaction with the processivity clamp potentiates Pol IV-mediated TLS

Seungwoo Chang, Luisa Laureti, Elizabeth S Thrall, Marguerite S Kay, Gaëlle Philippin, Slobodan Jergic, Vincent Pagès, Joseph Loparo

PNAS RESEARCH ARTICLE | GENETICS

A bipartite interaction with the processivity clamp potentiates Pol IV-mediated TLS

Seungwoo Chang[a], Luisa Laureti[b], Elizabeth S. Thrall[a,1], Marguerite S. Kay[a,2], Gaëlle Philippin[b], Slobodan Jergic[c], Vincent Pagès[b,3], and Joseph J. Loparo[a,3]

Affiliations are included on p. 8.

Edited by Michael M. Cox, University of Wisconsin-Madison, Madison, WI; received October 18, 2024; accepted December 6, 2024 by Editorial Board Member Graham C. Walker

Processivity clamps mediate polymerase switching for translesion synthesis (TLS). All three *Escherichia coli* TLS polymerases interact with the β_2 processivity clamp through a conserved clamp-binding motif (CBM), which is indispensable for TLS. Notably, Pol IV also interacts weakly with the rim of the clamp through non-CBM residues. Ablating this "rim contact" in cells results in selective sensitivity to DNA-damaging agents, raising the question how the rim contact contributes to TLS. Here, we show that the rim contact is critical for TLS past a strong replication block but barely necessary for a weak blocking lesion. Within the in vitro reconstituted *E. coli* replisome, the rim mutation compromises Pol IV-mediated TLS past 3-deaza-methyl dA, a strong block, whereas barely affecting TLS past N^2-furfuryl dG, a weak block. Similar observations are also made in *E. coli* cells bearing a single copy of these lesions in the genome. At lesion-stalled replication forks, single-stranded DNA binding protein locally enriches Pol IV, enabling it to bind the low-affinity rim site. This interaction poises Pol IV to better compete with Pol III, the replicative polymerase, which competitively inhibits Pol IV from interacting with the clamp through its CBM. We propose that this bipartite clamp interaction enables Pol IV to rapidly resolve lesion-stalled replication at a strong block through TLS, which reduces damage-induced mutagenesis.

DNA replication | translesion synthesis | repriming | DNA damage response | mutagenesis

Significance

DNA lesions impede DNA replication, contributing to genome instability. In *Escherichia coli*, lesion-stalled replication can be resolved through translesion synthesis (TLS) or the reinitiation of DNA replication by repriming downstream of the lesion. The choice between these pathways significantly impacts damage-induced mutagenesis. During the DNA damage response, low-fidelity TLS polymerases are highly induced but selectively recruited to stalled forks. This process is finely regulated through multiple protein–protein interactions involving TLS polymerases and the replisome. Here, we describe how the *E. coli* replisome uses a weak, noncanonical interaction between its processivity clamp and Pol IV TLS polymerase to promote TLS at the fork, minimizing mutagenesis. The underlying mechanism may provide insights into how macromolecular complexes engage accessory factors only when required.

Translesion synthesis (TLS) is a universal mechanism that cells use to resolve lesion-stalled DNA replication (1, 2). TLS is primarily mediated by TLS polymerases, which can efficiently synthesize past various template lesions that block replicative polymerases. TLS polymerases are largely error-prone, and their activities in cells are regulated at multiple steps ranging from transcription to protein–protein interactions (PPIs). Among these PPIs, interactions of TLS polymerases with processivity factors are indispensable for TLS in cells (3, 4).

The *Escherichia coli* β_2 clamp is an extensively characterized processivity factor that retains many of the structural and regulatory features of replicative processivity factors across species (5, 6). The *E. coli* β_2 clamp is a homodimer, and each protomer has a binding cleft for conserved short peptides known as clamp binding motifs (CBMs). Clamp-interacting proteins (CLIPs) use these CBMs to interact with the β_2 clamp (Fig. 1 *A*, *Left*) (7–10). The DNA polymerases of *E. coli*, including all three TLS polymerases, Pol II, IV, and V, have CBM(s). Mutating these CBMs abolishes DNA synthesis in cells by these polymerases although these mutant polymerases retain wild-type polymerase activity, highlighting the importance of the CBM-clamp cleft interaction (4, 11).

Switching between bacterial replicative (Pol III) and TLS polymerases for TLS is mediated by the β_2 clamp. Underlying this polymerase switching is the dual interaction between Pol III and the β_2 clamp (12). Pol III is a trimeric complex (αεθ) of the α polymerase subunit, the ε exonuclease subunit, and the θ accessory subunit (13). Notably, the α and ε subunits have their own CBMs (CBMα and CBMε in Fig. 1 *A*, *Left* and *Middle*) (11, 14, 15), but CBMα interacts with the clamp with a much higher affinity than CBMε. During processive replication, the α and ε subunits simultaneously occupy both clefts of the β_2 clamp (14), preventing the interaction of TLS polymerases with the β_2 clamp (12, 14). However, upon lesion stalling, while Pol III remains associated with the β_2 clamp through the α subunit, the cleft occupied by the ε subunit becomes more accessible to TLS polymerases, allowing a TLS polymerase to bind to the β_2 clamp and mediate TLS past the lesion (12). This gatekeeping mechanism by the ε subunit is tuned to impose a limited kinetic window for TLS as weakening the clamp binding of the ε subunit increases TLS and vice versa (12). Persistent replication stalling due to failing TLS eventually leads

The authors declare no competing interest.

This article is a PNAS Direct Submission. M.M.C. is a guest editor invited by the Editorial Board.

[1]Present address: Department of Chemistry and Biochemistry, Fordham University, Bronx, NY 10458.

[2]Present address: Molecular and Cell Biology Graduate Program, Brandeis University, Waltham, MA 02453.

[3]To whom correspondence may be addressed. Email: vincent.pages@cnrs.fr or joseph_loparo@hms.harvard.edu.

This article contains supporting information online at https://www.pnas.org/lookup/suppl/doi:10.1073/pnas.2421471122/-/DCSupplemental.

Published February 24, 2025.

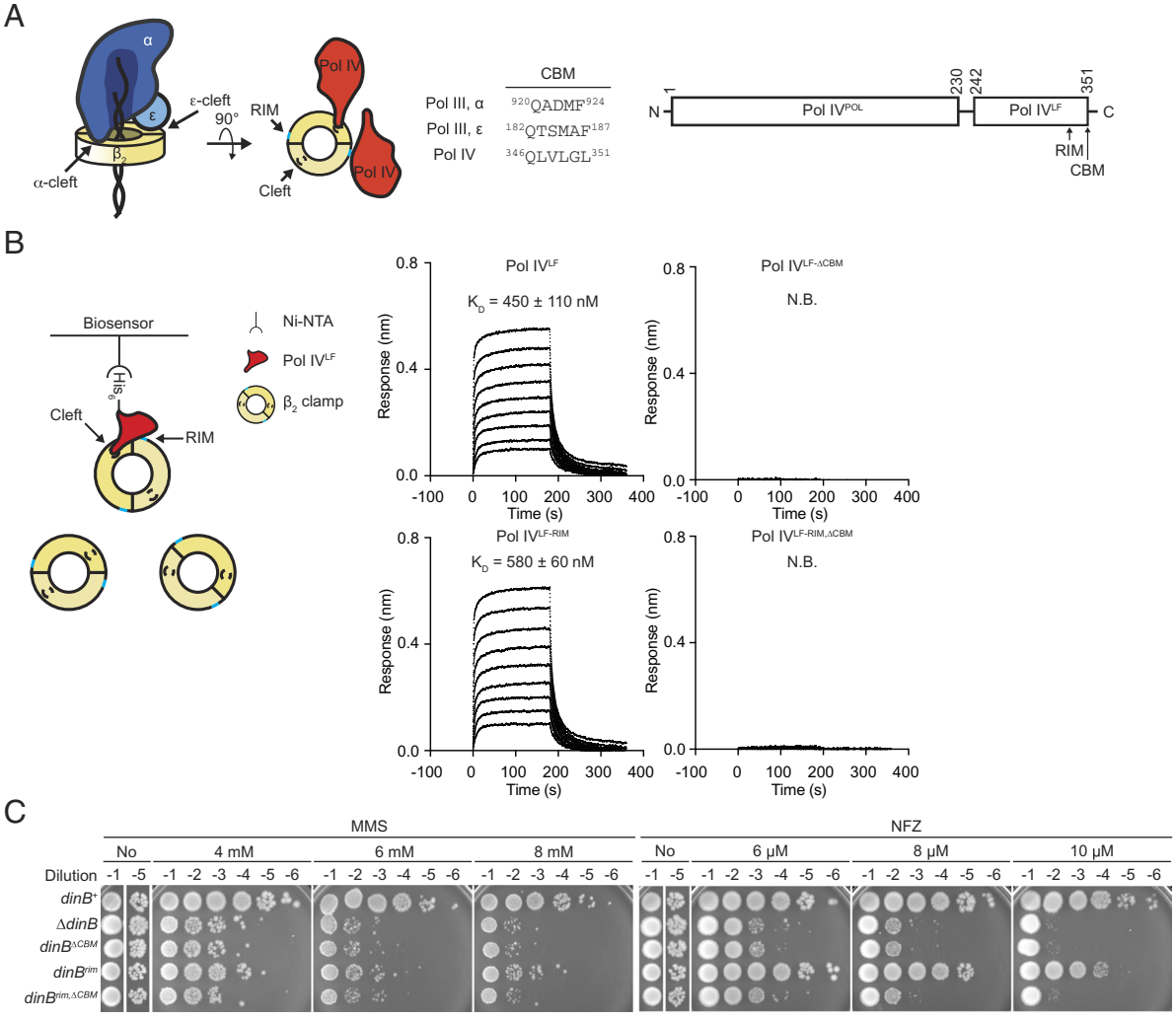

Fig. 1. *dinB*^{rim} is sensitized to damaging agents. (*A*, *Left*) Dual interaction of Pol III (αεθ) with the β_2 clamp through CBMs of α and ε subunits and bipartite interaction of Pol IV^{LF} with the β_2 clamp through the CBM and rim-interacting residues. (*Middle*) CBM sequences of Pol III and Pol IV. (*Right*) A domain structure of Pol IV. Pol IV^{POL}, polymerase domain; Pol IV^{LF}, little finger domain; RIM, rim-interacting residues (^{303}VWP^{305}); CBM, clamp binding motif (^{346}QLVLGL^{351}). (*B*) Interaction of Pol IV^{LF} and β_2 clamp. (*Left*) Interaction between Pol IV^{LF} and β_2 clamp was measured by biolayer interferometry. Indicated Pol IV^{LF} was immobilized to the NTA sensors through the N-terminal His_6 tag and β_2 clamp was titrated up to 8 μM. (*Right*) Traces are responses in the presence of varying concentrations of β_2 clamp. Steady-state responses at given concentrations of β_2 clamp were used to calculate equilibrium dissociation constants (K_D) for the cleft. Shown are means and SD of three independent measurements. N.B., no binding. (*C*) Mutating the rim-interacting residues of Pol IV sensitizes cells to MMS and NFZ. *dinB*, Pol IV; *dinB*^{rim}, Pol IV with the rim-interacting residues mutated (^{303}VWP^{305} to ^{303}AGA^{305}); *dinB*$^{\Delta CBM}$, Pol IV lacking the CBM; *dinB*$^{rim,\ \Delta CBM}$, Pol IV with both *dinB*^{rim} and *dinB*$^{\Delta CBM}$ mutations. Similar observations were made at least three times.

to repriming of DNA replication. Therefore, the ε-cleft interaction plays a pivotal role in determining how stalled replication forks are resolved.

Despite the indispensable role of the β_2 clamp in mediating TLS, the localization of Pol IV, and potentially other TLS polymerases, to lesion-stalled replication forks requires interaction with fork-associated ssDNA binding protein (SSB) (16, 17). While SSB is constitutively associated with replication forks, Pol IV only becomes enriched within lesion-stalled replication forks (18). Remodeling of fork-associated SSB upon lesion stalling drives this selective enrichment, enabling Pol IV to overcome the ε kinetic barrier (16, 19).

Interestingly, DNA polymerases also make noncleft contacts with the β_2 clamp which may have regulatory roles (8, 20). Such a noncleft interaction was observed in a cocrystal structure of the β_2 clamp and the little finger domain of Pol IV (Pol IV^{LF}) (Fig. 1 *A*, *Right*) (8). This additional contact located on the rim side of the β_2 clamp, the "rim contact," consists of a hydrophobic pocket formed by ^{303}VWP^{305} of Pol IV^{LF} and L^{98} of the β_2 clamp sticking into the pocket. Prior studies (21–23), primarily with biochemical reconstitutions, have concluded that the rim interaction promotes polymerase switching. However, it remains unclear how such a weak interaction is used in cells and, interestingly, exerts vastly differential impacts on TLS, depending on the identity of the blocking lesion.

To address these issues, lesions representing weak and strong replication blocks were investigated through in vitro reconstitutions, bacterial genetics, and single-molecule cellular imaging. Within a biochemical reconstitution of the *E. coli* replisome, we demonstrate that the rim contact promotes Pol IV-mediated TLS by facilitating the interaction of Pol IV with the β_2 clamp through the CBM. Binding of Pol IV to the β_2 clamp through its CBM, which is indispensable, is competitively inhibited by the ε subunit of Pol III (12), and the rim contact enables Pol IV to better compete with the ε subunit of Pol III presumably by concentrating Pol IV in close proximity to the cleft. Dependence of Pol IV-mediated TLS on the rim contact becomes more critical for a strong replication block, providing an explanation for selective sensitivity of the rim mutant to DNA-damaging agents. Intriguingly, the rim contact is too weak for the interaction with the β_2 clamp at cellular concentrations of Pol IV, and the defective

TLS resulting from ablating the rim interaction is corrected simply by elevating the level of Pol IV in cells. In addition, imaging results suggest that the rim interaction depends on SSB-mediated enrichment of Pol IV at lesion-stalled replication forks. We propose that Pol IV is enriched at stalled replication forks through the interaction with SSB, which drives formation of the rim interaction, promoting TLS.

Materials and Methods

Chemicals. Anhydrotetracycline (aTc, TaKaRa, 631310), ATPγS (Abcam, AB138911), dNTPs (New England Biolabs, N0446S), N,N-Dimethyl formamide anhydrous (Sigma, 227056), Formaldehyde (Sigma, F8775), Methyl methanesulfonate (MMS, Sigma, 129925), and Nitrofurazone (NFZ, Fluka, PHR1196) and rNTPs (New England Biolabs, N0450S).

Construction of Strains. The *E. coli* strains used in this study are all based on MG1655 and were created as described previously (12, 16). Briefly, recombineering strains bearing pSIM6 (24) were transformed with PCR-amplified dsDNA fragments containing an antibiotic selection marker and a desired modification(s). To construct a fluorescent SOS reporter strain, a cassette consisting of the promoter of *sulA* (−69 to −1 of *sulA*), the coding sequence for GFPmut2 (25) and *frt-kan-frt* (*sulAp-gfp-mut2-frt-kan-frt*) was inserted into the *E. coli* genome at the lambda attachment site (12, 26). In some cases, modified genomic loci were transferred into recipient strains by P1 transduction. From antibiotic-selected transformants, genomic regions containing the desired modifications were PCR amplified and sequenced. To flip out selection markers, cells were transformed with pCP20, which expresses a flippase, and the removal of a selection marker was confirmed by PCR. Construction of the parental strains for the pathway choice assay was described previously (27, 28).

Proteins. *E. coli* replication proteins were purified as described previously: Pol III clamp loader complex ($\tau_3\delta\delta'\chi\psi$) (29), Pol III core ($\alpha\varepsilon\theta$) (30), DnaB helicase (31), DnaG primase (32), β_2 sliding clamp (33) and SSB (34). Full-length wild-type Pol IV and its variants were expressed in BL21(DE3) *dinB::frt-kan-frt* and purified as described previously (35). PK-His6-tagged Pol IV^{LF} (Pol IV^{LF}: a.a. 243 to 351 of Pol IV with MGLRRASVHHHHHHSSGHIEGRHM appended to the N terminus) and its variants were expressed in Rosetta2 and purified using Ni-NTA resins. Eluates from Ni-NTA resins were further purified by size exclusion chromatography with a Superose 6 increase 10/300 GL column (Cytiva). Purified PK-His6-Pol IV^{LF} and its variants were stored in a storage buffer (50 mM Hepes-NaOH, pH8/100 mM NaCl/5% glycerol/10 mM 2-mercaptoethanol).

Sensitivity to DNA-Damaging Agents. Overnight cultures grown in LB at 30 °C with aeration were 10-fold serially diluted (from OD_{600} = 0.1) in LB and spotted onto LB agar plates containing NFZ or MMS, and anhydrous tetracycline (aTc) when overexpression of proteins of interest was needed.

Western Blotting. The expression levels of Pol IV-FLAG and Pol IV^{RIM}-FLAG were measured by Western blot as described previously (16). Overnight cultures grown in LB at 37 °C with aeration were diluted into fresh LB to $OD_{600} \approx 0.1$ and incubated at 37 °C with aeration until OD_{600} reached about 0.5. Then, MMS (final 7.5 mM) or a mock was added to the culture and cultures were further incubated at 37 °C with aeration for 1 h before cells were harvested. Cell lysates were prepared by lysing cells in B-PER™ (Thermo Scientific™) supplemented with Benzonase nuclease (Novagen, #70746) and EDTA-free protease inhibitor cocktail (Roche, #04693159001) and, based on OD_{600} at the time of harvest, an equal number of cells were loaded and run on an SDS-PAGE gel (Bio-Rad #4561086: 4–15 Mini-PROTEAN TGX) along with Precision Plus Protein Dual Color Standards (BIO-RAD, 1610374). Resolved proteins on an SDS-PAGE gel were transferred to a polyvinylidene difluoride membrane (PerkinElmer, #NEF1002001PK: PolyScreen PVDF Hybridization Transfer Membrane). After blocked in PBST containing 5% skim milk, the membrane was probed with a rabbit anti-FLAG polyclonal antibody raised against the antigen Ac-C(dPEG4)DYKDDDDK-OH (a gift of Johannes Walter, Department of Biological Chemistry and Molecular Pharmacology, Blavatnik Institute, Harvard Medical School, Boston, MA, USA). A goat anti-rabbit IgG-HRP antibody (Jackson ImmunoResearch, #111-035-003) was used as a secondary antibody. The membrane and chemiluminescent signals were visualized using an Amersham Imager 600 with HyGLO chemiluminescent HRP antibody detection reagent (Denville Scientific, #E2400).

In Vitro Reconstitution of Pol IV-Mediated TLS. Rolling circle templates were constructed as described previously (12, 16). Pol IV-mediated TLS was reconstituted within the *E. coli* replisome as described previously (12). Briefly, a lesion-containing rolling circle template (1 nM) was mixed with $DnaB_6$ (50 nM), $\tau_3\delta\delta'\chi\psi$ (20 nM), β_2 clamp (20 nM), Pol III core (60 nM), ATPγS (50 μM), dCTP/dGTP (each 60 μM) in 50 mM Hepes-KOH (pH8) on ice and incubated at 37 °C for 6 min. Then, replication was initiated by the addition of a prewarmed 10 X mixture of SSB_4 (500 nM), DnaG (100 nM), ATP (1 mM), CTP/GTP/UTP (each 250 μM), [α-^{32}P]-dATP. Ten seconds after the addition of the initiation mixture, a mock or Pol IV was added to the reactions and the reactions continued at 37 °C for 12 min. Reactions were quenched by the addition of EDTA (24 mM). Concentrations are all final in the replication reactions. Replication products were resolved in a 0.6% denaturing alkaline agarose gel and visualized by autoradiography. From the autoradiograph, relative abundance of the replication products at the resolution limit (RL) was quantified using ImageJ.

Measuring the Interaction between Pol IV and β_2 Clamp by Biolayer Interferometry. Purified PK-His6-Pol IV^{LF} and its variants were immobilized onto Octet NTA biosensors (Sartorius, 18–5103) and incubated with varying concentrations of β_2 clamp (31.3 to 8,000 nM as a dimer). Immobilization and binding reactions took place in binding buffer (50 mM Hepes-NaOH, pH7.5/100 mM NaCl/5 mM β-mercaptoethanol/0.05% Tween20). Shifts in the interference pattern upon interaction between Pol IV^{LF} and β_2 clamp were measured in real-time using Octet RED384 (Sartorius). To determine equilibrium dissociation constants, a one-site total binding model was fitted to the background (responses to β_2 clamp in the absence of immobilized Pol IV^{LF})-subtracted steady-state responses at varying concentrations of β_2 clamp. One-site total binding model: $R = Rmax \times A/(K_D + A) + NS \times A + Background$. R, response; Rmax, maximum response; A, concentration of analyte; NS, slope of nonspecific binding; Background, response in the absence of analytes.

Measuring the Damage-Induced SOS Responses. LB medium was inoculated with SOS reporter strains and incubated at 37 °C overnight with aeration. The overnight cultures were diluted in fresh LB to OD_{600} 0.1 and incubated at 37 °C with aeration until OD_{600} reached between 0.2 and 0.3. These cultures were treated with NFZ (60 μM, dissolved in dimethyl formamide) or MMS (7.5 mM) and further incubated at 37 °C with aeration for 1 h. Then, cells were collected by centrifugation and washed with ice-cold phosphate-buffered saline (PBS) twice. Washed cells were fixed with PBS containing 4% formaldehyde. Fixed cells were washed with ice-cold PBS twice and resuspended in ice-cold PBS. Fluorescence signals from individual cells were measured using a flow cytometer (BD Accuri C6). Means and SD of fluorescence signals from about one hundred thousand cells were determined.

Measuring Pathway Choice in Cells. Construction of control and lesion-containing plasmids: Plasmids carrying a single lesion for genomic integration were constructed as described previously (28). Briefly, 3-dMeA-containing and its lesion-free control plasmids were constructed by inserting an oligomer [5′-GCAAGTTAACACG-3′, A, 3-deaza-methyl dA (lesion) or dA (control)] into a gapped-duplex pGP1/2 (amp^R), creating an in-frame *lacZ* gene. N^2-furfuryl dG-containing and its lesion-free control plasmids were similarly created with lesion-containing and control oligomers [5′-CTACCTGTGGACGGCTGCGA-3′, G, N^2-furfuryl dG (lesion) or dG (control)] as described previously (16).

In-cell pathway choice assays: Assays were performed as described previously (28). Briefly, a control or lesion-containing plasmid was introduced into the recipient strains together with a transformation control plasmid (pVP146, tet^R) by electroporation using GenePulser Xcell (BioRad). These electroporated cells were first resuspended in 1 mL of super optimal broth with catabolic repressor (SOC), then 500 μL of resuspended cells was transferred into 2 mL of LB containing 0.2 mM IPTG to induce the expression of integrase and excisionase. These cells were further incubated at 37 °C for 45 min. A portion of these cells were plated on LB containing 10 μg/mL tetracycline to measure the transformation efficiency, and the rest of the cells were plated on LB containing ampicillin (50 μg/mL) and X-gal (80 μg/mL) to select for integrants (amp^R) and monitor TLS among the integrants (*lacZ*$^+$ phenotype, formation of sectored blue/white colonies in the presence of

X-gal). After 24-h incubation at 37 °C, colonies were counted, and choices of DA (white colony counts/total colony counts) and TLS (sectored blue-white colony counts/total colony counts) were determined.

Imaging. Samples were prepared for microscopy and imaged exactly as described previously (18). In brief, imaging cultures were grown in supplemented M9 medium with 0.4% glucose as the carbon source. IPTG was added to a final concentration of 0.5 mM to induce expression of the SSB-mYPet fusion. When cultures reached $OD_{600} \approx 0.15$, an aliquot was harvested by centrifugation and deposited on an agarose pad containing 100 mM MMS, which was sandwiched between cleaned coverslips. The sample was incubated on the pad for 20 min before imaging.

Imaging was performed in a custom-built fluorescence microscope described previously (18). A Nikon TE2000 microscope was equipped with a Nikon CFI Apo ×100/1.49 NA TIRF objective, dichroic mirrors and bandpass filters (Chroma), and a Hamamatsu ImageEM C9100-13 EMCCD camera. Excitation was provided by 514 nm and 561 nm lasers (Coherent Sapphire) and PAmCherry photoactivation was achieved using a 405 nm laser (Coherent OBIS). Lasers were focused to the objective back focal plane to achieve highly inclined thin illumination (36). Computer-controlled shutters were used to automate excitation sequences and the 405 nm photoactivation power was adjusted to control the density of photoactivated Pol IV-PAmCherry molecules. For all experiments, at least three different biological replicates (imaging cultures) were imaged on at least two different days.

Analysis of microscopy data was performed exactly as described previously (18). In brief, brightfield images of cells were segmented using the MicrobeTracker package (37) and detection and tracking of Pol IV-PAmCherry molecules was performed using the u-track package (38, 39). Pol IV-PAmCherry molecules were fit to 2D Gaussian approximations of the point spread function (PSF) and static molecules were identified based on their PSF width. For analysis of SSB-mYPet foci, the first five frames of 514 nm excitation were averaged and then spot detection was performed using u-track. To remove a small number of poorly fit weak fluorescent spots, foci with background values less than the camera offset level (1,500 counts) were removed. To avoid possible crosstalk from the SSB-mYPet foci, the small fraction of cells containing a Pol IV-PAmCherry localization in the first frame of PALM excitation were excluded from the dataset.

Colocalization between Pol IV-PAmCherry molecules and SSB-mYPet foci was analyzed using radial distribution function analysis exactly as described previously (18). The distance between each Pol IV-PAmCherry trajectory and the nearest SSB-mYPet focus in the cell was calculated and aggregated across all cells, giving an experimental distance distribution. Subsequently, Pol IV-PAmCherry localizations were randomly simulated in the cells and a random distance distribution was generated. The experimental distance distribution was normalized by the simulated one to give the radial distribution function $g(r)$ for all distance values r. This procedure was repeated for 100 simulated distance distributions and the resulting $g(r)$ curves were averaged to give the final average $g(r)$ curve. To validate the analysis, a separate random distance distribution was generated, and the same procedure was followed to generate an average random $g(r)$ curve; this random $g(r)$ curve should be approximately equal to one at all distances.

Results

Mutating the Rim-Interacting Residues Compromises Pol IV-Mediated TLS in Cells. In order to examine how the rim contact contributes to the interaction between Pol IV and the β_2 clamp, we set up a biolayer interferometry (BLI)-based binding assay (40). In this assay, Pol IV^{LF} was immobilized onto Ni-NTA-coated BLI sensors through an N-terminal His_6 epitope, and the interaction of Pol IV^{LF} with β_2 clamp was detected by BLI (Fig. 1 *B*, *Left*). Wild-type Pol IV^{LF} interacted with the β_2 clamp with an equilibrium dissociation binding constant (K_D) of ~450 nM (Fig. 1 *B*, *Right*), which is similar to the binding affinity measured by surface plasmon resonance with surface-immobilized β_2 clamp (21). Mutating the rim-interacting residues (^{303}VWP^{305} to AGA) within Pol IV (Pol IV^{RIM}) only marginally weakened this interaction (Fig. 1 *B*, *Right*), indicating that the rim contact is very weak. Furthermore, the rim interaction became measurable only in the presence of an intact CBM as deleting the CBM (Pol $IV^{\Delta CBM}$ and Pol $IV^{RIM,\Delta CBM}$) completely abolished the Pol IV-β_2 clamp interaction (Fig. 1 *B*, *Right*). These results suggest that while the rim interaction potentially promotes the CBM-β_2 clamp interaction, the rim interaction by itself is too weak to be measured.

Strikingly, however, the strain bearing the *dinB^{rim}* mutation was highly sensitized to methyl methanesulfonate (MMS), a Pol IV cognate damaging agent, only slightly less than the *ΔdinB* strain (Fig. 1*C* and *SI Appendix*, Table S1) (41, 42). Methylated bases in MMS-treated *E. coli* cells (3-methyl adenine and 7-methyl guanine) are either repaired by the base excision repair (BER) system or spontaneously depurinate, forming abasic sites (43–45). Given *E. coli* strains lacking *tag* and *alkA* (glycosylases for BER of 3-MeA) are highly sensitized to MMS, which is further exacerbated by the deletion of *dinB* (42), the increased sensitivity of *ΔdinB* and *dinB^{rim}* likely reflects defective TLS past 3-MeA. In stark contrast, the *dinB^{rim}* strain was only modestly sensitized to nitrofurazone (NFZ), another Pol IV cognate damaging agent (Fig. 1*C* and *SI Appendix*, Table S1). The *dinB^{rim}* strain retained normal damage-induced SOS responses including the induction of Pol IV (*SI Appendix*, Fig. S1 *A* and *B*), ruling out the possibility that the increased sensitivity results from defective damage responses. In addition, the *dinB$^{\Delta CBM}$*, which is as sensitized as the *ΔdinB* mutant, was epistatic to *dinB^{rim}* (Fig. 1*C* and *SI Appendix*, Table S1), indicating that the increased sensitivity of the *dinB^{rim}* strain is due to defective Pol IV-mediated TLS. These results suggest that the rim interaction promotes Pol IV-mediated TLS in cells and its contribution to TLS varies depending upon the lesion identity.

The Rim Interaction Is Critical for TLS Past 3-MeA. To understand the mechanistic basis of differential sensitivity of the *dinB^{rim}* to NFZ and MMS, we reconstituted TLS in vitro within the *E. coli* replisome (12, 46). This reconstitution uses rolling circle DNA templates that bear on the leading strand template N^2-furfuryl dG (N^2-FFdG) or 3-deaza-methyl dA (3-dMeA) (Fig. 2*A*), which are structural analogs of major DNA lesions created in NFZ- and MMS-treated *E. coli* cells, respectively (35, 47); here 3-dMeA was used instead of 3-methyl dA (3-MeA) due to the limited in vitro stability of 3-MeA (48–50). In the absence of Pol IV, reconstituted replisomes only poorly replicated the N^2-FFdG- and 3-dMeA-containing templates (No Pol IV in Fig. 2*B*), indicating that these are potent replication blocks for Pol III, the replicative polymerase (12, 16). Addition of Pol IV to the replication reactions promoted the synthesis of both leading and lagging strands with leading strand replication products accumulating at the RL of the gel [(1) and (2) in Fig. 2*B*] before Pol III-mediated replication is completely inhibited at higher concentrations of Pol IV (*SI Appendix*, Fig. S2*B*) (12, 16, 51, 52). Given that leading strand replication products accumulating at the RL result from more than 5 passages through blocking lesions without strand discontinuities such as nicks and gaps (*SI Appendix*, Fig. S2*A*), these results show that Pol IV can mediate TLS past these lesions within stalled replisomes (TLS at the fork) (12).

Our prior work with similar in vitro reconstitutions demonstrated that Pol IV is only briefly engaged in replication, primarily during the synthesis past a blocking lesion, while most of the replication is mediated by Pol III (12). When corrected for the replication-inhibitory effects of Pol IV (*SI Appendix*, Fig. S2*B*), maximum TLS past N^2-FFdG and 3-dMeA was achieved around 150 and 300 nM Pol IV respectively [(3) and (4) in Fig. 2*B*]. In addition, Pol IV-promoted replication of the N^2-FFdG-containing

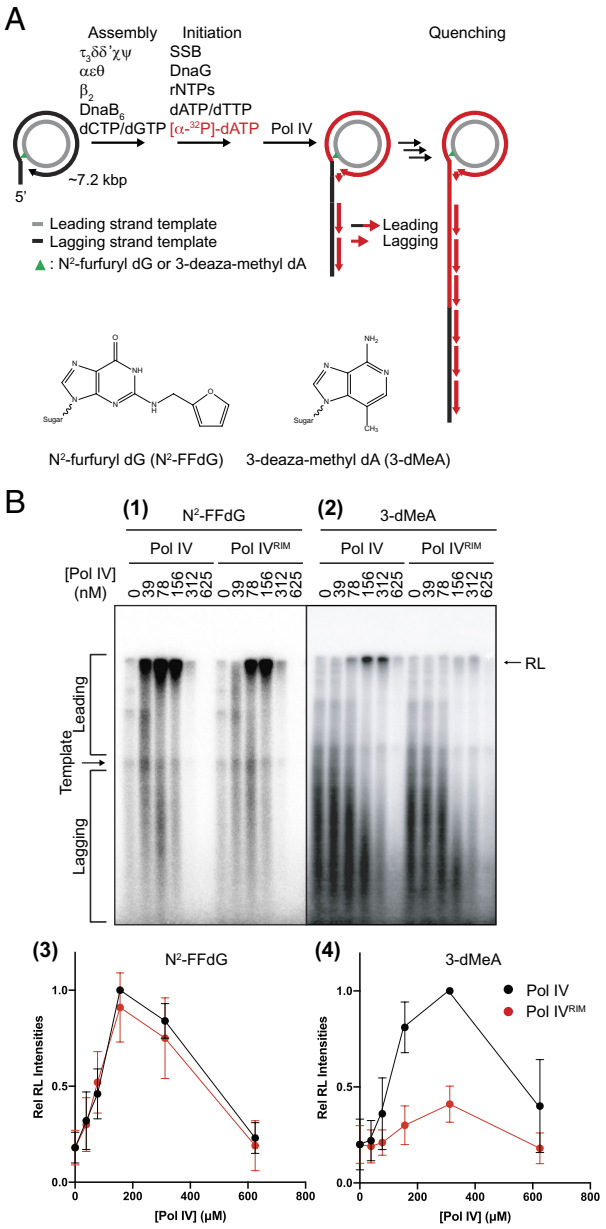

Fig. 2. The rim interaction promotes polymerase switching within lesion-stalled replisome. (*A*) A schematic of in vitro reconstituted Pol IV-mediated TLS. The inner circle (gray) is the leading strand template. Replication products are resolved in denaturing agarose gels and visualized by autoradiography as shown in (*B*). (*B*) Reconstitution of Pol IV-mediated TLS past N^2-FFdG [(1) and (3)] and 3-dMeA [(2) and (4)]. Indicated amounts of Pol IV or Pol IV^{RIM} were added to the replication reactions on the lesion-containing rolling circle templates. RL, resolution limit of the gel, ~45 kilonucleotides. Discrete bands between RL and template represent replication stalling (*SI Appendix*, Fig. S2*A*) and disappear in the presence of Pol IV. To calculate "Rel RL Intensities," intensities of the resolution-limited (RL) replication products from lesion-containing templates [as shown in (*A*), (1) and (2)] were first corrected for the impact of Pol IV or Pol IV^{RIM} on processive replication (as shown in *SI Appendix*, Fig. S2*B*) and then normalized to the highest intensity for each blocking lesion. Shown are means and SD of three to five independent measurements.

template resulted in more leading strand replication products than that of the 3-dMeA-containing template did (Fig. 2*B*). Collectively, these results indicate that Pol IV-mediated TLS is less efficient within 3-dMeA-stalled replication forks than it is within N^2-FFdG-stalled replication forks.

Notably, Pol IV^{RIM} barely promoted the replication of the 3-dMeA-containing template [(2) and (4) in Fig. 2*B*] whereas Pol IV^{RIM} promoted replication of the N^2-FFdG-containing template only slightly less efficiently as compared with Pol IV [(1) and (3) in Fig. 2*B*]. Together with Pol $IV^{\Delta CBM}$, which completely failed to promote TLS past N^2-FFdG in our in vitro reconstitution (*SI Appendix*, Fig. S2*C*), these differential impacts of the rim interaction on in vitro reconstituted TLS correlate well with the sensitivity of the corresponding *dinB* strains to NFZ and MMS (Fig. 1*C*). Therefore, we concluded that the rim interaction promotes TLS within lesion-stalled replisomes but plays a critical role only for strong replication blocks, such as 3-MeA.

Cooperative Interaction of Pol IV with SSB and β_2 Clamp. How the weak rim interaction robustly promotes the action of Pol IV within stalled replication forks remains unclear. Our prior work demonstrated that SSB highly enriches Pol IV at lesion-stalled replication forks, promoting formation of Pol IV-β_2 clamp complexes (16). To examine whether the rim interaction contributes to the formation of Pol IV-β_2 clamp complexes, we imaged individual Pol IV molecules localized at the fork in strains that express Pol IV-PAmCherry (Fig. 3 *A*, *Top*) and SSB-mYPet as previously described (Fig. 3 *A*, *Bottom*) (18). Briefly, we set the imaging conditions to selectively detect static Pol IV molecules, most of which represent Pol IV molecules forming complexes with SSB or the β_2 clamp at lesion-stalled forks in MMS-treated cells (16). Shown in Fig. 3 *B* and *C*, radial distribution values [g(r)] represent the relative abundance of these complexes at a distance (radius) from the fork (radius = 0) relative to chance (*SI Appendix*, Fig. S3*A*); random cellular localization is characterized by g(r) = 1 at all radius values, whereas g(r) > 1 indicates enrichment relative to chance. Deleting the CBM (Pol $IV^{\Delta CBM}$) caused a substantial reduction in the formation of Pol IV-β_2 clamp complexes at the fork [g(r) = 5.7 ± 0.1, mean ± SEM here and thereafter] as compared with wild-type Pol IV [g(r) ~ 8.0 ± 0.3] (Fig. 3*B* and *SI Appendix*, Fig. S3*B*). This reduction was slightly less than our previous measurement with Pol $IV^{RIM,\Delta CBM}$ [g(r) ~ 5] (16), indicating that the CBM is the major contributor to the formation of Pol IV-β_2 clamp complexes. Consistent with this idea, mutating only the rim interacting residues (Pol IV^{RIM}) led to a small but discernable reduction [g(r) = 7.0 ± 0.1] (Fig. 3*B* and *SI Appendix*, Fig. S3*B*). However, when SSB-mediated fork enrichment of Pol IV was diminished by the $dinB^{T120P}$ mutation (16), the $dinB^{rim}$ mutation (Pol $IV^{T120P,RIM}$) did not reduce the Pol IV-β_2 clamp interaction [g(r) = 3.3 ± 0.1] (Fig. 3*C* and *SI Appendix*, Fig. S3*C*) compared with our previous measurement with Pol IV^{T120P} [g(r) ~ 3] (16); combining the $dinB^{T120P}$ mutation with deletion of the CBM (Pol $IV^{T120P,\Delta CBM}$) completely ablated complex formation [g(r) = 0.47 ± 0.01] (Fig. 3*C* and *SI Appendix*, Fig. S3*C*). Collectively, these results suggest that the rim interaction is utilized within lesion-stalled replication forks but only when Pol IV is highly enriched by SSB.

In contrast to its high enrichment in MMS-treated cells, Pol IV is only slightly enriched at the fork in NFZ-treated cells (18), and the $dinB^{T120P}$ strain is only modestly sensitized to NFZ (Fig. 3*D* and *SI Appendix*, Table S1) (16), suggesting that relatively low enrichment is sufficient for Pol IV to mediate TLS past weak replication blocks such as structural analogs of N^2-FFdG. Notably, even though ablating the interaction of Pol IV with either SSB ($dinB^{T120P}$) or the rim ($dinB^{rim}$) only modestly sensitized cells to NFZ, ablating both the SSB and the rim interactions ($dinB^{T120P,rim}$) severely sensitized cells to NFZ (Fig. 3*D* and *SI Appendix*, Table S1). These results suggest that the rim promotes TLS past weak replication block as well, but its impact is much smaller. We propose that although the rim contact by itself is intrinsically very weak (Fig. 1*B*), SSB-mediated enrichment of Pol IV within stalled replication forks drives the rim interaction, further concentrating Pol IV near the β_2 clamp.

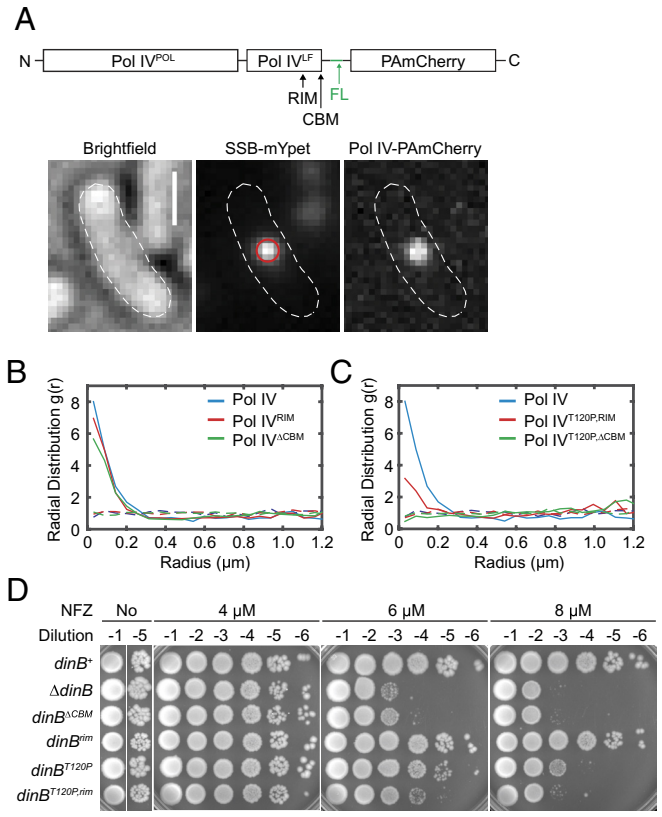

Fig. 3. Cooperative interaction of Pol IV with SSB and β_2 clamp at the fork. (*A*) A schematic of Pol IV-PAmCherry fusion (*Top*) and representative micrographs of an imaging strain (*Bottom*). (*Top*) Pol IV-PAmCherry. Pol IV^{POL}, polymerase domain; Pol IV^{LF}, little finger domain; RIM, rim-interacting residues, (^{303}VWP^{305}); CBM, clamp binding motif (^{346}QLVLGL^{351}); FL, flexible linker $(G_4S)_4$. (*Bottom*) Transmitted white light micrograph of single *E. coli* cell with cell outline and 1 μm scale bar (*Left*), fluorescence micrograph of single SSB-mYPet focus with overlaid centroid (*Middle*), and fluorescence micrograph of single Pol IV-PAmCherry molecule (*Right*). (*B*) Radial distribution function g(r) analysis of Pol IV in cells treated with 100 mM MMS for 20 min for (B) Pol IV^{WT} (N = 1,436), Pol IV^{RIM} (N = 3,905), and Pol IV$^{\Delta CBM}$ (N = 3,753) and (*C*) Pol IV^{WT} (N = 1,436), Pol IV^{T120P,RIM} (N = 1,881), and Pol IV$^{T120P,\Delta CBM}$ (N = 2,958). N, number of static Pol IV molecules included in the analysis. (*D*) Sensitivity to NFZ of the indicated strains. Similar observations were made three times.

The Rim Interaction Facilitates the CBM–Cleft Interaction. Interaction of Pol IV with β_2 clamp through its CBM is indispensable for TLS (Fig. 1*C* and *SI Appendix*, Fig. S2*C*) (16). However, this interaction is competitively inhibited by the ε subunit of Pol III, which acts as a gatekeeper at the replication fork (12). To see whether the rim interaction helps Pol IV overcome this gatekeeping mechanism, we examined the effect of strengthening the interaction between the ε subunit and the β_2 clamp on Pol IV-mediated TLS in cells. Consistent with our prior work (12), strengthening the interaction with the ε_L mutation in *dnaQ* (14) (Fig. 4*A*; see also Fig. 1*A*), which enhances the gatekeeping mechanism (12), modestly sensitized the cells to NFZ (Fig. 4*B* and *SI Appendix*, Table S1). This sensitization reflects suppressed Pol IV-mediated TLS because *dinB*$^{\Delta CBM}$ was epistatic to *dnaQ*(ε_L) (Fig. 4*B* and *SI Appendix*, Table S1). Notably, *dinB*^{rim} with the *dnaQ*(ε_L) background [*dnaQ*(ε_L) *dinB*^{rim}] was highly sensitized to NFZ even though *dinB*^{rim} with *dnaQ*$^{+}$ background (*dnaQ*$^{+}$ *dinB*^{rim}) was only modestly sensitized (Fig. 4*B* and *SI Appendix*, Table S1). These results suggest that the rim interaction enables Pol IV to better compete with the ε subunit.

Next, we tested whether loss of the rim interaction could be compensated for by elevating the expression of Pol IV^{RIM} in cells above its native levels. However, like Pol IV, elevated levels of Pol IV^{RIM} inhibited Pol III-mediated processive replication (*SI Appendix*, Fig. S2*B*), resulting in lethality (No NFZ in Fig. 4*C* and *SI Appendix*, Fig. S4 and Table S1) (52, 53). Therefore, we leveraged the *dinB*^{T120P} background, which substantially attenuates such lethality (No NFZ in Fig. 4*C* and *SI Appendix*, Fig. S4 and Table S1) (16, 41). Elevating the expression level of Pol IV^{T120P,RIM} in *dnaQ*(ε_L) Δ*dinB* made the cells more tolerant to NFZ (compare –aTc and +aTc in Fig. 4*C* and *SI Appendix*, Fig. S4 and Table S1), even more than *dnaQ*(ε_L) *dinB*^{rim} [compare *dnaQ*(ε_L) *dinB*^{rim} and *dnaQ*(ε_L) Δ*dinB ptet-dinB*^{T120P,rim} in Fig. 4*C* and *SI Appendix*, Fig. S4 and Table S1]. These results indicate that the role of the rim interaction is concentrating Pol IV near the β_2 clamp. In addition, elevating the expression level of Pol IV^{T120P} in *dnaQ*(ε_L) Δ*dinB* made the strain even more tolerant to NFZ compared with that of Pol IV^{T120P,RIM} (Fig. 4*C* and *SI Appendix*, Table S1). These results support the model that Pol IV is sequentially concentrated near the β_2 clamp by its interactions with SSB and the rim.

The Impact of the Rim Interaction on the Pathway Choice of Lesion-Stalled Replication. To directly examine whether the rim interaction promotes TLS in cells, we employed a genetic assay by which resolution of lesion-stalled replication through TLS or damage avoidance (DA) is quantified (28). Briefly, a single replication blocking lesion is integrated into the leading strand template of the *E. coli* genome (Fig. 5 *A*, *Left*, and *SI Appendix*, Fig. S5), and the resolution pathway choice in individual cells is determined by the color of the resulting colonies on X-gal plates (Fig. 5 *A*, *Right*). In the *dinB*$^{+}$ strain, 3-dMeA-stalled replication was primarily resolved by TLS (~80%) while only a small fraction (~20%) was through DA, which reflects repriming and subsequent homology-directed gap repair (Fig. 5*B* and *SI Appendix*, Table S1). Consistent with Pol IV being the major TLS polymerase for 3-MeA, deletion of Pol IV (Δ*dinB*) resulted in a substantial increase in DA (~95%) (Fig. 5*C*). In the *dinB*^{rim} mutant, resolution through TLS was reduced by ~20% with a concomitant increase in resolution through DA, indicating that the rim interaction indeed promotes Pol IV-mediated TLS in cells. This reduction is smaller than the impact of the *dinB*^{rim} mutation on in vitro reconstituted TLS past 3-dMeA (Fig. 2*B*). However, it should be noted that our rolling circle-based assay amplifies reductions in TLS because the reduction accumulates over multiple passages through the blocking lesion. As our cell-based assay is single passage, both the in cell and the in vitro observations are consistent. In the *dinB*$^{+}$ strain, N^2-FFdG-stalled replication was also primarily resolved through TLS (~60%) (Fig. 5*C* and *SI Appendix*, Table S1) (16). In stark contrast to TLS past 3-dMeA, however, TLS past N^2-FFdG was not reduced in the *dinB*^{rim} mutant (Fig. 5*B* and *SI Appendix*, Table S1), which is consistent with our in vitro results (Fig. 2*B*). Additionally, in the Δ*dinB* background, in which TLS can be inefficiently mediated by Pol III (16), TLS-mediated resolution of 3-dMeA-stalled replication was only ~7% whereas that of N^2-FFdG-stalled replication was ~40%, indicating that 3-dMeA is a much stronger replication block for Pol III than N^2-FFdG (Fig. 5*C* and *SI Appendix*, Table S1). Collectively, these results demonstrate that the rim interaction indeed promotes TLS-mediated resolution of lesion-stalled replication in cells and plays a more pronounced role for a stronger replication block.

Discussion

Hierarchical Protein–Protein Interactions for Utilization of TLS Polymerases. The rim interaction was initially observed in a cocrystal structure of the little finger domain of Pol IV (Pol IV^{LF}) and the β_2 clamp (8). In the structure, the C-terminal end of Pol IV^{LF}, which contains the CBM, adopts a stretched conformation,

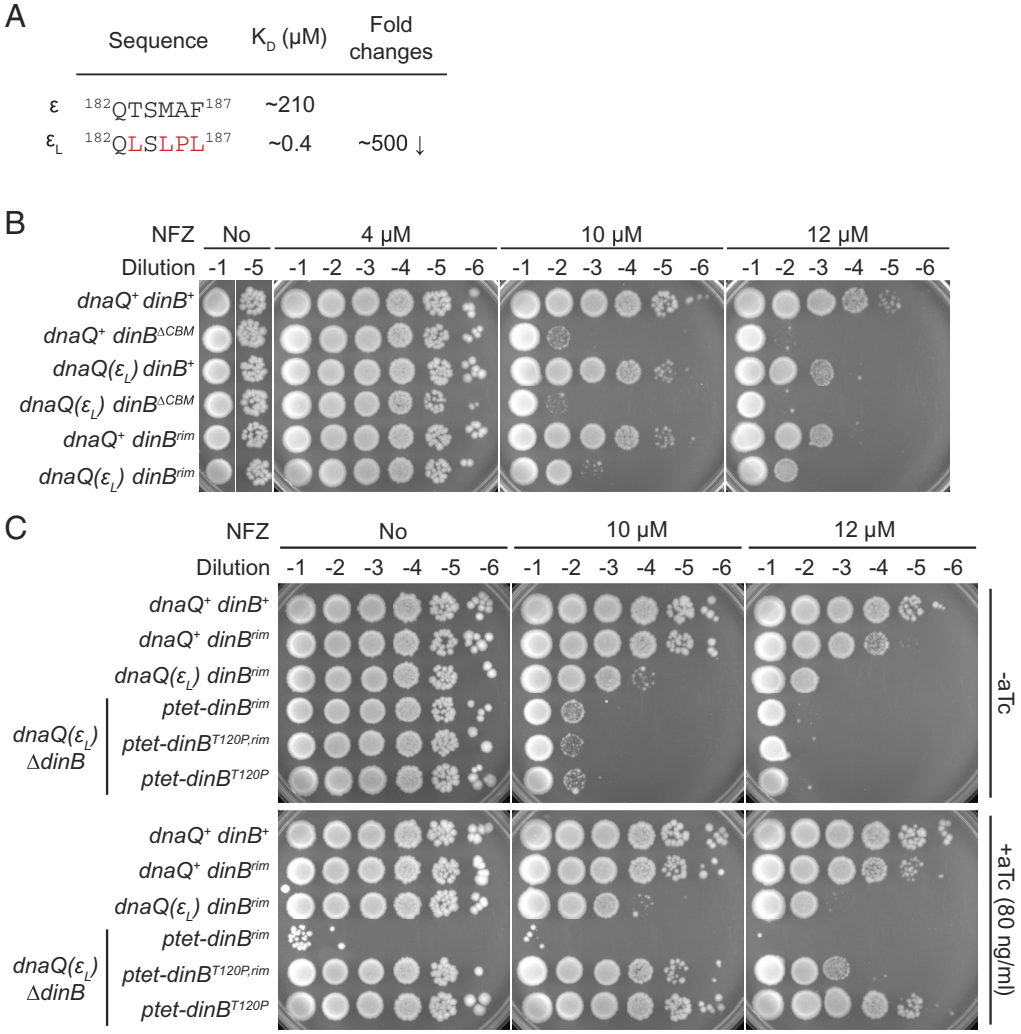

Fig. 4. The rim interaction potentiates the CBM–cleft interaction. (*A*) A CBM mutation in the ε subunit that strengthens the ε-clamp interaction. (*B*) Sensitivity to NFZ of the indicated strains. Similar observations were made three times. (*C*) Elevating the expression of Pol IV^{RIM} in *dnaQ(ε$_L$) ΔdinB* normalizes tolerance to NFZ. Indicated Pol IV variants were ectopically expressed from a Tet-inducible expression cassette engineered in the *E. coli* genome. aTc, anhydrotetracycline. Similar observations were made three times.

which allows Pol IV^{LF} to simultaneously contact both a cleft and the adjacent rim. Given that the rim interaction is extremely weak on its own (Fig. 1*B*), it has remained unclear whether it has physiological relevance or is merely an artifact of crystallization conditions. How do cells use such a weak interaction? Our findings indicate that at lesion-stalled replication forks, SSB enriches Pol IV (16, 18, 19) enough to drive the weak rim interaction. The resulting transient but frequent interaction at the rim potentially poises Pol IV to more efficiently bind to the adjacent cleft, which is competitively inhibited by Pol III and possibly other clamp-interacting proteins (12, 16). This competitive advantage imparted by the rim interaction becomes more important for lesions that are difficult to bypass.

As inferred from the cocrystal structure, a strong rim interaction would keep the polymerase domain away from the Primer/Template junction (8), preventing Pol IV-mediated synthesis. Indeed, *dinB^{rim}* mutations tested by others (^{303}VWP^{305} to AGA or SGA) slightly increased β_2 clamp-supported primer extension by Pol IV (21, 41, 53). Moreover, a strong rim interaction would allow Pol IV to occupy the cleft more potently, inhibiting Pol III-mediated processive replication (12, 22, 51). Therefore, in conjunction with the selective enrichment of Pol IV at stalled forks by SSB (12, 16), a weak rim interaction promotes Pol IV-mediated TLS while minimally inhibiting processive replication.

The Role for Pol IV-Mediated TLS in Damage-Induced Mutagenesis. MMS-induced mutagenesis serves as a good model for how different TLS polymerases are utilized during the resolution of lesion-stalled replication. 3-methyladenine, a major methyl adduct in MMS-treated cells, is a cognate lesion of Pol IV, yet MMS-induced mutagenesis requires *umuDC*, the gene encoding Pol V (54). This Pol V-dependent mutagenesis is highly increased upon deletion of *dinB* (42). As with other leading strand lesions, methyl adduct-stalled replisomes can reprime DNA replication downstream of the blocking lesion (16), which leaves a ssDNA gap (55, 56). These gaps can be filled in by postreplicative synthesis involving Pol V, a highly mutagenic TLS polymerase (57). Our prior work demonstrated that Pol IV can mediate TLS within lesion-stalled replisomes (TLS at the fork), preventing replisomes from repriming (12). In MMS-treated *ΔdinB*, it is likely that lesion-stalled replisomes more frequently reprime, resulting in elevated mutagenesis (41, 42). In *dinB^{rim}*, the MMS-induced SOS response (*SI Appendix*, Fig. S1*B*), which reflects the generation of ssDNA gaps, and MMS-induced mutagenesis are both elevated, but less so compared to *ΔdinB* (41). These observations are consistent with the rim interaction promoting Pol IV-mediated TLS at the fork in cells which suppresses damage-induced mutagenesis.

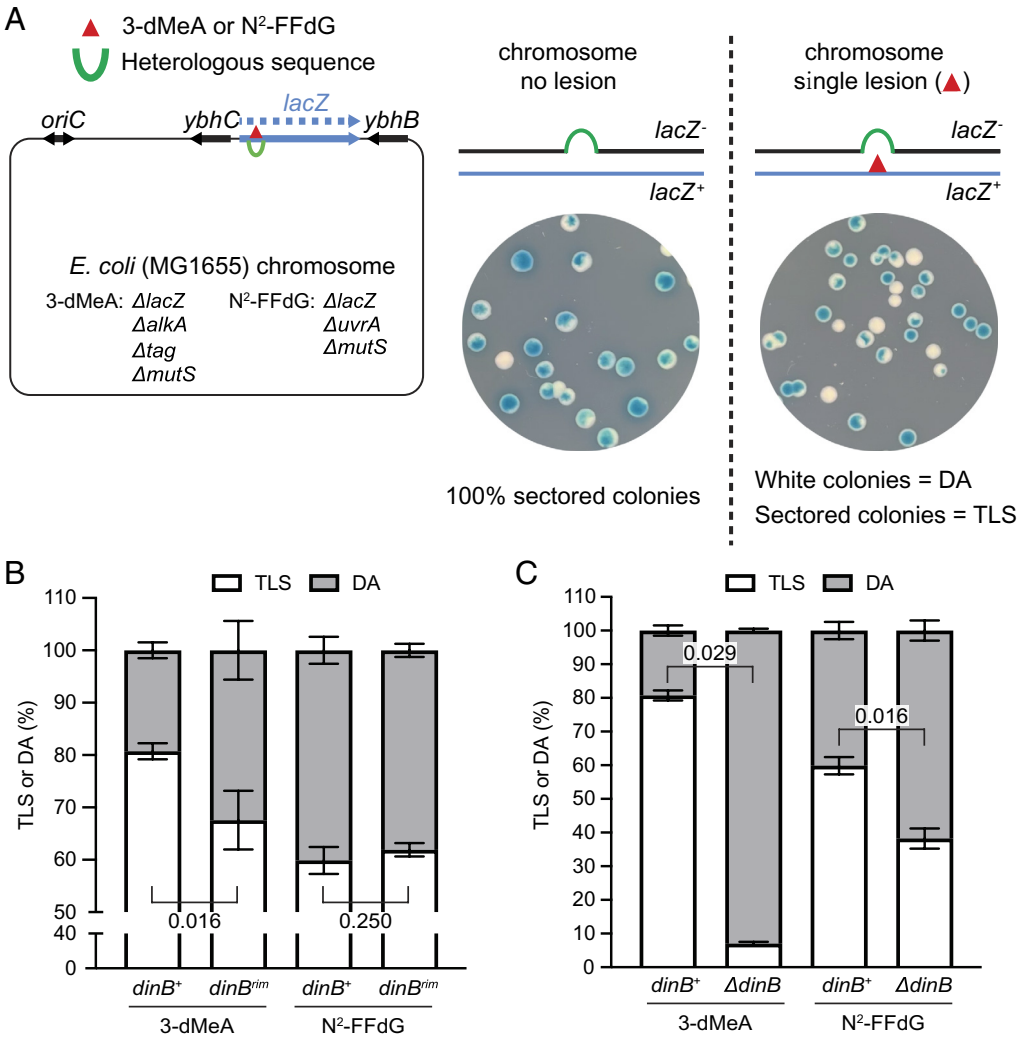

Fig. 5. Pathway choice of lesion-stalled replication in cells. (*A*) Quantification of pathway choice between TLS and DA in cells. (*Left*) The assay strain is based on *E. coli* MG1655 and the genome was engineered as shown in the diagram. To prevent the genome-incorporated lesions from being removed by repair pathways, base excision (*alkA* and *tag*) or nucleotide excision (*uvrA*) repair was inactivated together with the inactivation of the mismatch repair (*mutS*). (*Right*) On X-gal plates, resolution of lesion-stalled replication through DA in a cell results in the formation of a white colony whereas resolution through TLS results in the formation of a blue-sectored colony. Note that functional LacZ is expressed only when stalled replication is resolved by TLS. In this study, blocking lesions were introduced into the leading strand template in the *E. coli* genome. All the results presented here are based on at least three measurements with independently prepared materials. (*B*) Pathway choice of lesion-stalled replication in $dinB^{+}$ and $dinB^{rim}$. Shown are means and SD of three to five independent measurements. *P* values for the indicated comparison pairs were calculated with the Mann–Whitney and Wilcoxon matched-pairs test. (*C*) Contribution of Pol IV to TLS-mediated resolution of lesion-stalled replication. Shown are means and SD of four to five independent measurements.

In light of damage-induced mutagenesis, what is the benefit of having this ancillary protein–protein interaction? Our results suggest that the rim interaction allows for more efficient TLS at the fork without high induction of Pol IV, which can inhibit DNA replication and repriming, thus preventing rapid resolution of lesion-stalled replication.

Possible Roles for Ancillary Clamp Interactions of DNA Polymerases. All DNA polymerases of *E. coli*, except for Pol I, contain conserved CBMs (7), which are indispensable for their functions in cells (4, 58). However, it is possible that like Pol IV, these polymerases also make secondary contacts with the β_2 clamp that modulate the CBM-β_2 clamp interaction. For example, Pol III, the replicative DNA polymerase, makes additional contacts with the β_2 clamp and ablating these interactions impair the action of Pol III (20, 59, 60). Given the impact of the secondary clamp interaction of Pol IV on damage-induced mutagenesis, it would be interesting to discover such auxiliary clamp interactions for other TLS polymerases.

Data, Materials, and Software Availability. The datasets from the current study are available in a Zenodo repository (DOI: 10.5281/zenodo.14624467) (61). The custom MATLAB code used in this study is available in a Zenodo repository (DOI: 10.5281/zenodo.7007581) (62).

ACKNOWLEDGMENTS. We thank K. Arnett (Center for Macromolecular Interactions, Harvard Medical School) for assistance with the BLI experiments, N. Dixon (University of Wollongong) for feedback on our manuscript, and D. Li (University of Rhode Island) for providing the N²-FFdG-containing oligomer. This work was supported by NIH grants R01 GM114065 (to J.J.L.) and F32 GM113516 (to E.S.T.), The William F. Milton Fund (to S.C.), Fondation pour la Recherche Médicale Equipe FRM-EQU201903007797 (to V.P.).

Author affiliations: [a]Department of Biological Chemistry and Molecular Pharmacology, Blavatnik Institute, Harvard Medical School, Boston, MA 02115; [b]Cancer Research Center of Marseille: Team DNA Damage and Genome Instability | CNRS, Aix Marseille Université, Inserm, Institut Paoli-Calmettes, Marseille F-13009, France; and [c]School of Chemistry and Molecular Bioscience, Molecular Horizons, University of Wollongong, Wollongong, NSW 2522, Australia

Author contributions: S.C., L.L., E.S.T., V.P., and J.J.L. designed research; S.C., L.L., E.S.T., M.S.K., and G.P. performed research; S.C., L.L., E.S.T., G.P., and S.J. contributed new reagents/analytic tools; S.C., L.L., E.S.T., M.S.K., V.P., and J.J.L. analyzed data; and S.C., L.L., E.S.T., M.S.K., G.P., S.J., V.P., and J.J.L. wrote the paper.

1. R. P. Fuchs, S. Fujii, Translesion DNA synthesis and mutagenesis in prokaryotes. *Cold Spring Harb. Perspect. Biol.* **5**, a012682 (2013).
2. K. T. Powers, M. T. Washington, Eukaryotic translesion synthesis: Choosing the right tool for the job. *DNA Repair* **71**, 127–134 (2018).
3. Z. Zhuang, Y. Ai, Processivity factor of DNA polymerase and its expanding role in normal and translesion DNA synthesis. *Biochim. Biophys. Acta* **1804**, 1081–1093 (2010).
4. O. J. Becherel, R. P. P. Fuchs, J. Wagner, Pivotal role of the β-clamp in translesion DNA synthesis and mutagenesis in E. coli cells. *DNA Repair (Amst)* **1**, 703–708 (2002).
5. J. Kuriyan, M. O'Donnell, Sliding clamps of DNA polymerases. *J. Mol. Biol.* **234**, 915–925 (1993).
6. C. Indiani, M. O'Donnell, The replication clamp-loading machine at work in the three domains of life. *Nat. Rev. Mol. Cell Biol.* **7**, 751–761 (2006).

7. A. A. Patoli, J. A. Winter, K. A. Bunting, The UmuC subunit of the E. coli DNA polymerase V shows a unique interaction with the β-clamp processivity factor. *BMC Struct. Biol.* **13**, 12 (2013).
8. K. A. Bunting, S. M. Roe, L. H. Pearl, Structural basis for recruitment of translesion DNA polymerase Pol IV/DinB to the β-clamp. *EMBO J.* **22**, 5883–5892 (2003).
9. F. J. L. de Saro, M. O'Donnell, Interaction of the β sliding clamp with MutS, ligase, and DNA polymerase I. *Proc. Natl. Acad. Sci. U.S.A.* **98**, 8376–8380 (2001).
10. B. P. Dalrymple, K. Kongsuwan, G. Wijffels, N. E. Dixon, P. A. Jennings, A universal protein–protein interaction motif in the eubacterial DNA replication and repair systems. *Proc. Natl. Acad. Sci. U.S.A.* **98**, 11627–11632 (2001).
11. P. R. Dohrmann, C. S. McHenry, A bipartite polymerase-processivity factor interaction: Only the internal β binding site of the α subunit is required for processive replication by the DNA polymerase III holoenzyme. *J. Mol. Biol.* **350**, 228–239 (2005).
12. S. Chang *et al.*, A gatekeeping function of the replicative polymerase controls pathway choice in the resolution of lesion-stalled replisomes. *Proc. Natl. Acad. Sci. U.S.A.* **116**, 25591–25601 (2019).
13. C. S. McHenry, W. Crow, DNA polymerase III of Escherichia coli. Purification and identification of subunits. *J. Biol. Chem.* **254**, 1748–1753 (1979).
14. S. Jergic *et al.*, A direct proofreader–clamp interaction stabilizes the Pol III replicase in the polymerization mode. *EMBO J.* **32**, 1322–1333 (2013).
15. A. T. Rêgo, A. N. Holding, H. Kent, M. H. Lamers, Architecture of the Pol III–clamp–exonuclease complex reveals key roles of the exonuclease subunit in processive DNA synthesis and repair. *EMBO J.* **32**, 1334–1343 (2013).
16. S. Chang *et al.*, Compartmentalization of the replication fork by single-stranded DNA-binding protein regulates translesion synthesis. *Nat. Struct. Mol. Biol.* **29**, 932–941 (2022).
17. A. Furukohri, Y. Nishikawa, M. T. Akiyama, H. Maki, Interaction between Escherichia coli DNA polymerase IV and single-stranded DNA-binding protein is required for DNA synthesis on SSB-coated DNA. *Nucleic Acids Res.* **40**, 6039–6048 (2012).
18. E. S. Thrall, J. E. Kath, S. Chang, J. J. Loparo, Single-molecule imaging reveals multiple pathways for the recruitment of translesion polymerases after DNA damage. *Nat. Commun.* **8**, 2170 (2017).
19. E. S. Thrall, S. C. Piatt, S. Chang, J. J. Loparo, Replication stalling activates SSB for recruitment of DNA damage tolerance factors. *Proc. Natl. Acad. Sci. U.S.A.* **119**, e2208875119 (2022).
20. R. Fernandez-Leiro, J. Conrad, S. H. Scheres, M. H. Lamers, cryo-EM structures of the E. coli replicative DNA polymerase reveal its dynamic interactions with the DNA sliding clamp, exonuclease and τ. *Elife* **4**, e11134 (2015).
21. J. M. H. Heltzel, R. W. Maul, S. K. S. Ponticelli, M. D. Sutton, A model for DNA polymerase switching involving a single cleft and the rim of the sliding clamp. *Proc. Natl. Acad. Sci. U.S.A.* **106**, 12664–12669 (2009).
22. J. E. Kath *et al.*, Polymerase exchange on single DNA molecules reveals processivity clamp control of translesion synthesis. *Proc. Natl. Acad. Sci. U.S.A.* **111**, 7647–7652 (2014).
23. C. B. Gabbai, J. T. P. Yeeles, K. J. Marians, Replisome-mediated translesion synthesis and leading strand template lesion skipping are competing bypass mechanisms. *J. Biol. Chem.* **289**, 32811–32823 (2014).
24. S. Datta, N. Costantino, D. L. Court, A set of recombineering plasmids for gram-negative bacteria. *Gene* **379**, 109–115 (2006).
25. B. P. Cormack, R. H. Valdivia, S. Falkow, FACS-optimized mutants of the green fluorescent protein (GFP). *Gene* **173**, 33–38 (1996).
26. J. D. McCool *et al.*, Measurement of SOS expression in individual Escherichia coli K-12 cells using fluorescence microscopy. *Mol. Microbiol.* **53**, 1343–1357 (2004).
27. E. Esnault, M. Valens, O. Espéli, F. Boccard, Chromosome structuring limits genome plasticity in Escherichia coli. *PLoS Genet.* **3**, e226 (2007).
28. V. Pagès, G. Mazón, K. Naiman, G. Philippin, R. P. Fuchs, Monitoring bypass of single replication-blocking lesions by damage avoidance in the Escherichia coli chromosome. *Nucleic Acids Res.* **40**, 9036–9043 (2012).
29. N. A. Tanner *et al.*, Single-molecule studies of fork dynamics in Escherichia coli DNA replication. *Nat. Struct. Mol. Biol.* **15**, 170–176 (2008).
30. J. S. Lewis *et al.*, Single-molecule visualization of fast polymerase turnover in the bacterial replisome. *Elife* **6**, e23932 (2017).
31. R. R. Spinks *et al.*, DnaB helicase dynamics in bacterial DNA replication resolved by single-molecule studies. *Nucleic Acids Res.* **49**, 6804–6816 (2021).
32. N. P. J. Stamford, J. Stamford, P. E. Lilley, N. E. Dixon, Enriched sources of Escherichia coli replication proteins. The dnaG primase is a zinc metalloprotein. *Biochim. Biophys. Acta* **1132**, 17–25 (1992).
33. A. J. Oakley *et al.*, Flexibility revealed by the 1.85 Å crystal structure of the β sliding-clamp subunit of Escherichia coli DNA polymerase III. *Acta Crystallogr. Sect. D: Biol. Crystallogr.* **59**, 1192–1199 (2003).
34. C. E. Mason *et al.*, Escherichia coli single-stranded DNA-binding protein: NanoESI-MS studies of salt-modulated subunit exchange and DNA binding transactions. *J. Am. Soc. Mass Spectrom.* **24**, 274–285 (2013).
35. D. F. Jarosz, V. G. Godoy, J. C. Delaney, J. M. Essigmann, G. C. Walker, A single amino acid governs enhanced activity of DinB DNA polymerases on damaged templates. *Nature* **439**, 225–228 (2006).
36. M. Tokunaga, N. Imamoto, K. Sakata-Sogawa, Highly inclined thin illumination enables clear single-molecule imaging in cells. *Nat. Methods* **5**, 159–161 (2008).
37. O. Sliusarenko, J. Heinritz, T. Emonet, C. Jacobs-Wagner, High-throughput, subpixel precision analysis of bacterial morphogenesis and intracellular spatio-temporal dynamics. *Mol. Microbiol.* **80**, 612–627 (2011).
38. K. Jaqaman *et al.*, Robust single particle tracking in live cell time-lapse sequences. *Nat. Methods* **5**, 695–702 (2008).
39. F. Aguet, C. N. Antonescu, M. Mettlen, S. L. Schmid, G. Danuser, Advances in analysis of low signal-to-noise images link dynamin and AP2 to the functions of an endocytic checkpoint. *Dev. Cell* **26**, 279–291 (2013).
40. T. Do *et al.*, A rapid method for determining dynamic binding capacity of resins for the purification of proteins. *Protein Expr. Purif.* **60**, 147–150 (2008).
41. M. K. Scotland *et al.*, A genetic selection for dinB mutants reveals an interaction between DNA polymerase IV and the replicative polymerase that is required for translesion synthesis. *PLoS Genet.* **11**, e1005507 (2015).
42. I. Bjedov *et al.*, Involvement of Escherichia coli DNA polymerase IV in tolerance of cytotoxic alkylating DNA lesions in vivo. *Genetics* **176**, 1431–1440 (2007).
43. M. D. Wyatt, J. M. Allan, A. Y. Lau, T. E. Ellenberger, L. D. Samson, 3-methyladenine DNA glycosylases: Structure, function, and biological importance. *Bioessays* **21**, 668–676 (1999).
44. P. D. Lawley, D. J. Orr, Specific excision of methylation products from DNA of Escherichia coli treated with N-methyl-N′-nitro-N-nitrosoguanidine. *Chem. Biol. Interact.* **2**, 154–157 (1970).
45. G. P. Margison, P. J. O'Connor, Biological implications of the instability of the N-glycosidic bone of 3-methyldeoxyadenosine in DNA. *Biochim. Biophys. Acta* **331**, 349–56 (1973).
46. C. A. Wu, E. L. Zechner, K. J. Marians, Coordinated leading- and lagging-strand synthesis at the Escherichia coli DNA replication fork. I. Multiple effectors act to modulate Okazaki fragment size. *J. Biol. Chem.* **267**, 4030–4044 (1992).
47. D. T. Beranek, C. C. Weis, D. H. Swenson, A comprehensive quantitative analysis of methylated and ethylated DNA using high pressure liquid chromatography. *Carcinogenesis* **1**, 595–606 (1980).
48. B. S. Plosky *et al.*, Eukaryotic Y-family polymerases bypass a 3-methyl-2′-deoxyadenosine analog in vitro and methyl methanesulfonate-induced DNA damage in vivo. *Nucleic Acids Res.* **36**, 2152–2162 (2008).
49. T. M. Cafarelli, T. J. Rands, V. G. Godoy, The DinB•RecA complex of Escherichia coli mediates an efficient and high-fidelity response to ubiquitous alkylation lesions. *Environ. Mol. Mutagenesis* **55**, 92–102 (2014).
50. T. Fujii, T. Saito, T. Nakasaka, Purines. XXXIV: 3-methyladenosine and 3-methyl-2′-deoxyadenosine: Their synthesis, glycosidic hydrolysis, and ring fission. *Chem. Pharm. Bull.* **37**, 2601 (2008).
51. C. Indiani, L. D. Langston, O. Yurieva, M. F. Goodman, M. O'Donnell, Translesion DNA polymerases remodel the replisome and alter the speed of the replicative helicase. *Proc. Natl. Acad. Sci. U.S.A.* **106**, 6031–6038 (2009).
52. K. Uchida *et al.*, Overproduction of Escherichia coli DNA polymerase DinB (Pol IV) inhibits replication fork progression and is lethal. *Mol. Microbiol.* **70**, 608–622 (2008).
53. J. Wagner, H. Etienne, R. P. Fuchs, A. Cordonnier, D. Burnouf, Distinct β-clamp interactions govern the activities of the Y family PolIV DNA polymerase. *Mol. Microbiol.* **74**, 1143–1151 (2009).
54. P. F. Schendel, M. Defais, The role of umuC gene product in mutagenesis by simple alkylating agents. *Mol. Gen. Genet.* **177**, 661–665 (1980).
55. J. T. P. Yeeles, K. J. Marians, The Escherichia coli replisome is inherently DNA damage tolerant. *Science* **334**, 235–238 (2011).
56. J. T. P. Yeeles, K. J. Marians, Dynamics of leading-strand lesion skipping by the replisome. *Mol. Cell* **52**, 855–865 (2013).
57. A. Isogawa, J. L. Ong, V. Potapov, R. P. Fuchs, S. Fujii, Pol V–Mediated translesion synthesis elicits localized untargeted mutagenesis during post-replicative gap repair. *Cell Rep.* **24**, 1290–1300 (2018).
58. N. Lenne-Samuel, J. Wagner, H. Etienne, R. P. P. Fuchs, The processivity factor β controls DNA polymerase IV traffic during spontaneous mutagenesis and translesion synthesis in vivo. *EMBO Rep.* **3**, 45–49 (2002).
59. M. H. Lamers, R. E. Georgescu, S.-G. Lee, M. O'Donnell, J. Kuriyan, Crystal structure of the catalytic alpha subunit of E. coli replicative DNA polymerase III. *Cell* **126**, 881–892 (2006).
60. C. Homiski *et al.*, The mutant βE202K sliding clamp protein impairs DNA polymerase III replication activity. *J. Bacteriol.* **203**, e0030321 (2021).
61. S. Chang *et al.*, A bipartite interaction with the processivity clamp potentiates Pol IV-mediated TLS. Zenodo. https://zenodo.org/records/14624468. Deposited 9 January 2025.
62. E. S. Thrall, S. C. Piatt, S. Chang, J. J. Loparo, Replication stalling activates SSB for recruitment of DNA damage tolerance factors. Zenodo. https://zenodo.org/record/7007581#.Yy2pBnZBy3A. Deposited 22 August 2022.